

# PERFORMANCE EVALUATION OF THREE-LEG VOLTAGE SOURCE INVERTER FED UNSYMMETRICAL TWO-PHASE INDUCTION MOTOR BASED ON GENETIC ALGORITHM FOR PARAMETER ESTIMATION

Prayad KONGSUK<sup>1</sup>, Vijit KINNARES<sup>1</sup>, Phunyaphat PHUMIPHAK<sup>2</sup>

<sup>1</sup>Department of Electrical Engineering, Faculty of Engineering,  
King Mongkut's Institute of Technology Ladkrabang, Chalongkrung Road, 10520 Bangkok, Thailand  
<sup>2</sup>Department of Electrical Engineering, Faculty of Engineering, Mahanakorn University of Technology,  
Cheum-Sampan Road 140, 10530 Bangkok, Thailand

pkongsuk@yahoo.com, kkwijit@kmitl.ac.th, kcthanaphiwat@yahoo.com

DOI: 10.15598/aece.v17i4.3405

**Abstract.** This paper presents an evaluation method of performance characteristics in terms of loss, currents and electromagnetic torque of an unsymmetrical two-phase induction motor driven by a three-leg Voltage Source Inverter (VSI) providing unbalanced two-phase voltages. The model parameters for consideration of loss and dynamic performance of the motor are estimated by using Genetic Algorithm (GA). Also, synthesized winding current waveforms based on a superposition method and frequency domain of known harmonic voltages are investigated. The methodology of the proposed GA applied to parameter estimation of the unsymmetrical two-phase induction motor is fully given. Carrier-based unbalanced Space Vector Pulse With Modulation (SVPWM) is employed and implemented on a low-cost microcontroller. In order to prove the validity of the model with the parameters obtained by GA, performance comparison with the experiment and the model with the parameters obtained by conventional test in laboratory has been made. The results of simulation with the proposed parameters and experiment are in good agreement.

## Keywords

*Genetic algorithm, parameter estimation, three-leg voltage source inverter, unsymmetrical two-phase induction motor.*

## 1. Introduction

Nowadays, Single-Phase Induction Motors (SPIMs) are commonly used for low power applications in domestic and industrial use such as pumps, fans, refrigerators, air conditioners, etc. because of low cost, ease of use and maintenance. However, these motors have several disadvantages such as low efficiency, low power factor and high torque ripple [1]. When supplied with a fixed frequency and fixed voltage power supply, they are essentially a constant speed motor. A wide range of speed is required for some applications like pumps, fans, and so on. A Voltage Source Inverter (VSI) with constant  $V \cdot \text{Hz}^{-1}$  is preferable in such variable speed drive systems. More importantly, the VSI for variable speed drives offers not only energy savings but also capability of soft start and stop. When supplied with the VSI, the capacitor run SPIMs having a capacitor connected together with an auxiliary winding will have a limitation of use because some frequencies at a low-frequency range of the VSI may cause a resonance problem resulting from interaction between the capacitor and the auxiliary winding [2]. As a consequence, winding damage may be present due to over current. Hence, if the variable speed drives of the SPIMs are required, it is necessary to modify the SPIM as a Two-Phase Induction Motor (TPIM) by removing the capacitor and supply with a three-leg VSI as shown in Fig. 1 ([1], [2], [3], [4], [17] and [18]). Performance like currents,  $V \cdot \text{Hz}^{-1}$  control of a TPIM driven by three-leg and four-leg VSIs with a carrier-based unbalanced PWM method has been compared and evaluated [4]. Also, publications [1], [2], [3], [4] and [5] have proved

superior performance of unbalanced two-phase voltages over balanced two-phase voltages supplied to the TPIM in terms of torque ripple and speed holding capability. However, loss analysis for a three-leg VSI-fed unsymmetrical TPIM has not been reported yet. Efficiency optimization control and loss analysis based on equivalent circuits of single-phase motor drives can be found in [6], [7], [8] and [9].

Recent parameter estimation methods of induction machines based on Genetic Algorithm (GA) have been reported in [10], [11], [12], [13], [14] and [22]. The estimating field efficiency and mechanical torque of an inverter-fed three-phase induction motor at various operating frequencies and loads use only a set of data from field measurement [10]. The data coupled with the use of GA is based on the modified motor equivalent circuit concept. However, the accuracy of the motor efficiency is moderate. In addition, the direct estimation of stray load losses of induction motors from the motor input parameters using GA-based parameter estimation methodology was presented by [15] and [16]. Loss measurement of an unsymmetrical induction motor for considering minimizing loss with adjustment of  $V \cdot \text{Hz}^{-1}$  level was proposed in [17]. From literature survey, GAs are only used to identify parameters for a three-phase induction motor. In the case of single-phase and unsymmetrical two-phase induction motors, there are a few publications. Therefore, accurate prediction of loss, currents, and electromagnetic torque using accurate model is required for motor design and control to meet achievement of high efficiency and good performance.

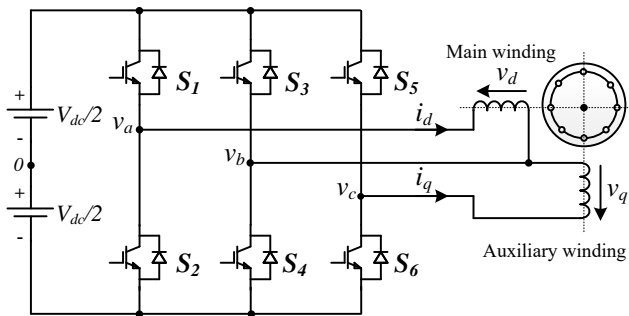


Fig. 1: Three-leg voltage source inverter supplying unsymmetrical TPIM.

The objective of this paper is to propose a parameter estimation method based on GA for loss model and dynamic model of the unsymmetrical TPIM when supplied by a three-leg VSI controlled with SVPWM. This paper is organized as follows. Firstly, loss model and dynamic model of the unsymmetrical TPIM based on equivalent circuits are fully given. Then, principle of carrier-based unbalanced voltage SVPWM is reviewed. The proposed GA applied to identification of equivalent circuit parameters is described. Synthesis of winding currents in time domain from frequency domain is

performed to verify the validity of parameters of the equivalent circuits. Results and discussion are given. Finally, conclusion is presented.

## 2. Two-Phase Induction Motor

### 2.1. Loss Model

The proposed loss model of an unsymmetrical TPIM is based on equivalent circuits for fundamental and harmonic frequencies taking into account core loss as shown in Fig. 2. The unsymmetrical TPIM parameters for the equivalent circuits can be achieved by standard test in laboratory, namely no-load test and blocked rotor test [19]. However in this paper, alternatively, the parameters for the modified equivalent circuits of the unsymmetrical TPIM are identified by GA in order to achieve more accurate values taking into account some effects such as saturation and skin effect.

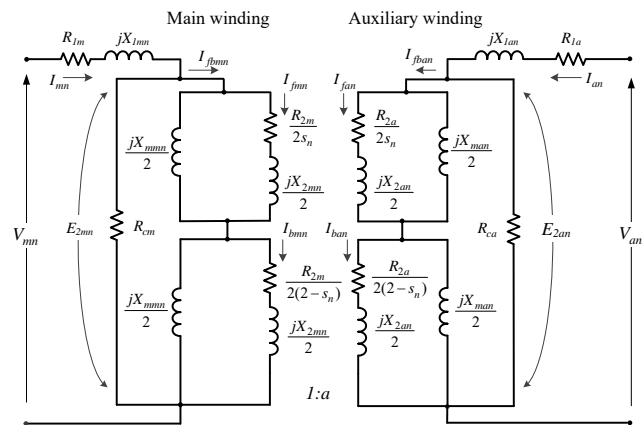


Fig. 2: Unsymmetrical TPIM equivalent circuit for determining fundamental frequency and harmonic losses.

Fundamental frequency and harmonic impedances of the main winding can be determined by the following equations:

$$Z_{mn} = Z_{1mn} + Z_{2mn}, \tag{1}$$

where

$$Z_{1mn} = (R_{1m} + jX_{1mn}), \tag{2}$$

and

$$Z_{2mn} = \frac{R_{cm} (Z_{fmn} + Z_{bmn})}{R_{cm} + (Z_{fmn} + Z_{bmn})}. \tag{3}$$

The impedances associated with the forward and backward magnetic fields are given by Eq. (4) and Eq. (5), respectively:

$$Z_{fmn} = \frac{\frac{jX_{mnmn}}{2} \left( \frac{R_{2m}}{2s_n} + j\frac{X_{2mn}}{2} \right)}{\frac{jX_{mnmn}}{2} + \left( \frac{R_{2m}}{2s_n} + j\frac{X_{2mn}}{2} \right)}, \tag{4}$$

$$Z_{bmn} = \frac{\frac{jX_{mnn}}{2} \left( \frac{R_{2m}}{2(2-s_n)} + j\frac{X_{2mn}}{2} \right)}{\frac{jX_{mnn}}{2} + \left( \frac{R_{2m}}{2(2-s_n)} + j\frac{X_{2mn}}{2} \right)}, \quad (5)$$

$$Z_{fbmn} = Z_{fmn} + Z_{bmn}, \quad (6)$$

$$Z_{2mn} = \frac{(Z_{fbmn}R_{cm})}{(Z_{fbmn} + R_{cm})}. \quad (7)$$

The main voltage and current equations for each harmonic of the circuit are:

$$V_{mn} = V_{1mn} + E_{2mn}, \quad (8)$$

$$I_{mn} = \frac{V_{mn}}{Z_{mn}}, \quad (9)$$

$$I_{fbmn} = \frac{I_{mn}R_{cm}}{Z_{fbmn} + R_{cm}}, \quad (10)$$

$$I_{fmn} = I_{fbmn} \frac{\frac{jX_{mnn}}{2}}{\frac{R_{2m}}{2s_n} + \frac{jX_{2mn}}{2} + j\frac{X_{mnn}}{2}}, \quad (11)$$

$$I_{bmn} = I_{fbmn} \frac{\frac{jX_{mnn}}{2}}{\frac{R_{2m}}{2(2-s_n)} + \frac{jX_{2mn}}{2} + j\frac{X_{mnn}}{2}}. \quad (12)$$

Similarly to the main winding, fundamental frequency and harmonic impedances of the auxiliary winding are given by the following equations:

$$Z_{an} = Z_{1an} + Z_{2an}, \quad (13)$$

where

$$Z_{1an} = (R_{1a} + jX_{1n}), \quad (14)$$

and

$$Z_{2an} = \frac{R_{ca} + (Z_{fan} + Z_{ban})}{R_{ca} (Z_{fan} + Z_{ban})}. \quad (15)$$

The impedances associated with the forward and backward magnetic fields of the auxiliary winding are given by Eq. (18) and Eq. (19), respectively:

$$Z_{fban} = Z_{fan} + Z_{ban}, \quad (16)$$

$$Z_{2an} = \frac{(Z_{fban}R_{ca})}{(Z_{fban} + R_{ca})}, \quad (17)$$

$$Z_{fan} = \frac{\frac{jX_{man}}{2} \left( \frac{R_{2a}}{2s_n} + j\frac{X_{2an}}{2} \right)}{\left( \frac{R_{2a}}{2s_n} + j\frac{X_{2an}}{2} \right) + j\frac{X_{2mn}}{2}}, \quad (18)$$

$$Z_{ban} = \frac{\frac{jX_{man}}{2} \left( \frac{R_{2a}}{2(2-s_n)} + j\frac{X_{2an}}{2} \right)}{\left( \frac{R_{2a}}{2(2-s_n)} + j\frac{X_{2a}}{2} \right) + j\frac{X_{man}}{2}}. \quad (19)$$

The auxiliary voltage and current equations for each harmonic of the circuit are:

$$V_{an} = aV_{mn}, \quad (20)$$

$$V_{an} = V_{1an} + E_{2an}, \quad (21)$$

$$I_{an} = \frac{V_{an}}{Z_{an}}. \quad (22)$$

For fundamental frequency and harmonic loss analysis, by using a superposition method, the harmonic equivalent circuit for each order  $n$  can be modified from the sinusoidal source as shown in Fig. 2. Harmonic slip can be expressed as:

$$s_n = \frac{n\omega_s - \omega_r}{n\omega_s}. \quad (23)$$

Total stator copper loss can be written as:

$$P_{Cus} = \sum_{n=1}^{\infty} I_{mn}^2 R_{1m} + I_{an}^2 R_{1a}. \quad (24)$$

Similarly, total rotor copper loss (i.e. the sum of the total copper loss for main and auxiliary winding circuits) can be calculated as:

$$P_{Cur} = P_{Curm} + P_{Cura}, \quad (25)$$

where

$$P_{Curm} = \sum_{n=1}^{\infty} \left( I_{fmn}^2 \frac{R_{2m}}{2s_n} + I_{bmn}^2 \frac{R_{2m}}{2(2-s_n)} \right), \quad (26)$$

$$P_{Cura} = \sum_{n=1}^{\infty} \left( I_{fan}^2 \frac{R_{2a}}{2s_n} + I_{ban}^2 \frac{R_{2a}}{2(2-s_n)} \right), \quad (27)$$

Total copper loss can be calculated as:

$$P_{Cu} = P_{Cus} + P_{Cur}. \quad (28)$$

Referring to the loss model, total core loss equation can be written as:

$$P_{Fe} = P_{Fem} + P_{Fca} = \sum_{n=1}^{\infty} \left( \frac{E_{2m}^2}{R_{cm}} + \frac{E_{2a}^2}{R_{ca}} \right). \quad (29)$$

Resistances  $R_{cm}$  and  $R_{ca}$  representing harmonic core loss in the main and auxiliary winding circuits, respectively, are assumed to be constant as the resistance representing the fundamental core loss.

Alternatively, the core loss can be expressed as follows:

$$P_{Fe} = P_h + P_e, \quad (30)$$

$$P_{Fe} = K_h f \Phi^2 + K_e f^2 \Phi^2, \quad (31)$$

$$P_{Fe} = \left( \frac{K_h}{f} + K_e \right) f^2 \Phi^2, \quad (32)$$

where  $K_h$  is the hysteresis coefficient;  $K_e$  is the classical eddy coefficient due to magnetic domain;  $\Phi$  is magnetic flux;  $f$  is the frequency of exciting voltage.

The input power of an electrical machine when the friction loss and stray load losses are negligible can be given as:

$$P_{in} = P_m + P_{Cus} + P_{Cur} + P_{Fe}. \quad (33)$$

## 2.2. Dynamic Model of Unsymmetrical Two-Phase Induction Motor

Since the equivalent circuit in Fig. 2 can be used only for calculation in steady state, dynamic model with direct and quadrature axes is required to achieve performance of dynamic response in terms of winding currents and electromagnetic torque. As mentioned earlier, the unsymmetrical TPIM was modified from an existing single-phase capacitor run induction motor by removing a capacitor out from an auxiliary winding. Two stator windings are displaced in space by 90 electrical degrees, known as main and auxiliary windings. Generally, both windings have different impedances. The equivalent circuits, representing the unsymmetrical TPIM in a stationary reference frame  $dq$  fixed in the stator where direct ( $d$ ) and quadrature ( $q$ ) axes denote the main and auxiliary windings, respectively, are shown in Fig. 3. The dynamic model equations of the unsymmetrical TPIM can be expressed as follows [1], [2], [3], [4] and [5]:

$$v_{sd}^s = R_{sd} i_{sd}^s + \frac{d\lambda_{sd}^s}{dt}, \quad (34)$$

$$v_{sq}^s = R_{sq} i_{sq}^s + \frac{d\lambda_{sq}^s}{dt}, \quad (35)$$

$$0 = R_r i_{rd}^s + \frac{d\lambda_{rd}^s}{dt} + \omega_r \lambda_{rq}^s, \quad (36)$$

$$0 = R_r i_{rq}^s + \frac{d\lambda_{rq}^s}{dt} + \omega_r \lambda_{rd}^s, \quad (37)$$

$$\lambda_{sd}^s = L_{sd} i_{sd}^s + M_{srd} i_{rd}^s, \quad (38)$$

$$\lambda_{sq}^s = L_{sq} i_{sq}^s + M_{srq} i_{rq}^s, \quad (39)$$

$$\lambda_{rd}^s = L_r i_{rd}^s + M_{srd} i_{sd}^s, \quad (40)$$

$$\lambda_{rq}^s = L_r i_{rq}^s + M_{srq} i_{sq}^s, \quad (41)$$

$$T_e = P \left( i_{sq}^s i_{rd}^s M_{srq} - i_{sd}^s i_{rq}^s M_{srd} \right), \quad (42)$$

$$P(T_m - T_e) = J \frac{d\omega_r}{dt} + B\omega_r. \quad (43)$$

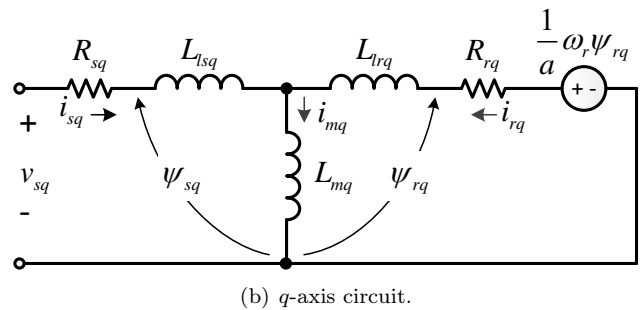
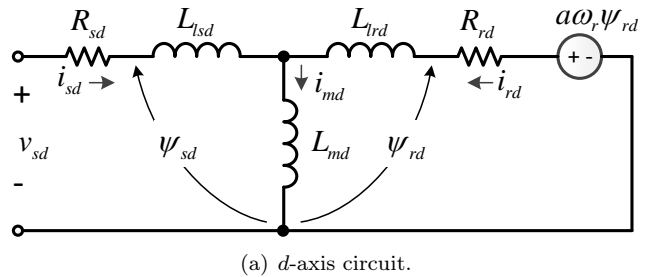


Fig. 3: Dynamic  $d$ - $q$  equivalent circuits of unsymmetrical TPIM.

Equation (34), Eq. (35), Eq. (36), Eq. (37), Eq. (38), Eq. (39), Eq. (40) and Eq. (41) are the general dynamic equations for a symmetrical TPIM which  $L_{sd} = L_{sq}$ ,  $M_{srd} = M_{srq}$  and  $R_{sd} = R_{sq}$ . In case of the asymmetry of the machine parameters where  $L_{sd} \neq L_{sq}$ ,  $M_{srd} \neq M_{srq}$  and  $R_{sd} \neq R_{sq}$ , electromagnetic torque ripple is present from supplying balanced voltages to both coils. The method for eliminating the torque ripple by controlling the stator currents is applied. Equation (34), Eq. (35), Eq. (36), Eq. (37), Eq. (38), Eq. (39), Eq. (40) and Eq. (41) are treated in terms of the rotor mutual flux:

$$\begin{aligned} T_e &= P \left( i_{sq}^s \left( \frac{\lambda_{rd}^s - M_{srd} i_{sd}^s}{L_r} \right) M_{msq} + \right. \\ &\quad \left. - i_{sd}^s \left( \frac{\lambda_{rq}^s - M_{srq} i_{sq}^s}{L_r} \right) M_{msd} \right) = \\ &= \frac{P}{L_r} \left( i_{sq}^s \lambda_{rd}^s M_{srq} - i_{sd}^s \lambda_{rq}^s M_{srd} \right), \end{aligned} \quad (44)$$

where  $i_{rd}^s = \frac{\lambda_{rd}^s - M_{srd} i_{sd}^s}{L_r}$  and  $i_{rq}^s = \frac{\lambda_{rq}^s - M_{srq} i_{sq}^s}{L_r}$ ,

$$T_e = \frac{P}{L_r} \left( i_{sq}^s \lambda_{rd}^s M_{srq} - i_{sd}^s \lambda_{rq}^s M_{srd} \right). \quad (45)$$

Then, the improved stator currents can be given as:

$$i_{sd}^{s'} = i_{sd}^s, \quad (46)$$

$$i_{sq}^{s'} = ai_{sq}^s, \quad (47)$$

where  $a = \frac{M_{srq}}{M_{srd}}$  and substituting the variables  $i_{sd}^s$  and  $i_{sq}^s$  by  $i_{sd}^{s'}$  and  $i_{sq}^{s'}$  respectively into Eq. (45), to remodel the torque as:

$$T_e = \frac{P}{L_r} \left( \frac{i_{sq}^{s'}}{a} \lambda_{rd}^s M_{srq} - i_{sd}^{s'} \lambda_{rq}^s M_{srd} \right) = \frac{P}{L_r} \left( \frac{M_{srd}}{M_{srq}} i_{sq}^{s'} \lambda_{rd}^s M_{srq} - i_{sd}^{s'} \lambda_{rq}^s M_{srd} \right), \quad (48)$$

$$T_e = \frac{PM_{srd}}{L_r} \left( i_{sq}^{s'} \lambda_{rd}^s - i_{sd}^{s'} \lambda_{rq}^s \right). \quad (49)$$

Equation (49) is identical to the symmetric machine which eliminates the oscillating term in the steady-state condition. It means that the magnitude of  $i_{sd}^{s'}$  is equal to that of  $i_{sq}^{s'}$ . The expression for the relation between current magnitudes of both windings for an asymmetrical parameter type is:

$$I_d = aI_q. \quad (50)$$

$I_q$  leads  $I_d$  by 90 electrical degrees. As regarding to the power balance, the relation of the supplied voltages for both windings is approximately as:

$$V_q = aV_d. \quad (51)$$

Note that  $V_q$  is normally greater than  $V_d$ .

### 2.3. Carrier Based Unbalanced SVPWM

The principle of the unbalanced carrier-based SVPWM can be illustrated in Fig. 4. Initially, the phase-leg reference signal waveforms for balanced two-phase outputs of SPWM (sinusoidal pulse width modulation) can be expressed as [3]:

$$v_{as} = m_a \sin(\omega t), \quad (52)$$

$$v_{bs} = m_a \sin(\omega t - 90^\circ), \quad (53)$$

$$v_{cs} = m_a \sin(\omega t - 180^\circ). \quad (54)$$

In order to achieve SVPWM providing unbalanced two-phase voltages, let

$$v_z = -\frac{\max(v_{as}, v_{bs}, v_{cs}) + \min(v_{as}, v_{bs}, v_{cs})}{2}. \quad (55)$$

Then, for SVPWM providing unbalanced two-phase outputs, the required phase-leg reference signal waveforms which are modified from SPWM can be expressed as:

$$v_a^* = m_a \sin(\omega t) + v_z, \quad (56)$$

$$v_b^* = m_a \sin(\omega t - 90^\circ + \delta) + v_z, \quad (57)$$

$$v_c^* = m_a \sin(\omega t - 180^\circ) + v_z. \quad (58)$$

The required reference signals for the main and auxiliary winding voltages are as follows:

$$v_d^* = v_a^* - v_b^*, \quad (59)$$

$$v_q^* = v_c^* - v_b^*. \quad (60)$$

The instantaneous fundamental voltages of the windings as shown in Fig. 4 can be expressed as:

$$V_{d1} = \overbrace{2m_a \sin\left(45^\circ - \frac{\delta}{2}\right)}^{\text{amplitude}} V_{dc} \cos\left(\omega t - 45^\circ + \frac{\delta}{2}\right), \quad (61)$$

$$V_{q1} = \overbrace{2m_a \cos\left(45^\circ - \frac{\delta}{2}\right)}^{\text{amplitude}} V_{dc} \cos\left(\omega t + 45^\circ + \frac{\delta}{2}\right). \quad (62)$$

Using the amplitudes of Eq. (58) and Eq. (59) yields:

$$\delta = 2 \tan^{-1}\left(\frac{1}{a}\right) - 90^\circ. \quad (63)$$

In this research work, turns ratio  $a$  is equal to 1.539 resulting in  $\delta = -23.97^\circ$ . According to Eq. (61) and Eq. (62), for given values of  $\delta$  and DC voltage, the magnitudes of both winding voltages are linearly proportional to the modulation index  $m_a$  for a linear range (i.e.  $0 \leq m_a \leq 1$ ). For V/F control, the modulation index is linearly proportional to the inverter frequency except at a low inverter frequency region. In order to achieve constant flux at this region, voltage boost is required. The profile of winding voltages against inverter frequency for this research work is shown in Fig. 5.

## 3. Methodology

### 3.1. Motor Parameter Estimation Using Genetic Algorithm

Genetic Algorithm (GA) is an enhancement technique which may be utilized to understand an arrangement of nonlinear equation. It utilizes target capacities taking into account some execution standard to ascertain a mistake. On the other hand, the GA is in light of natural selection and natural genetics quality utilizing random numbers, and does not oblige a decent starting evaluation. The mechanics of the hereditary

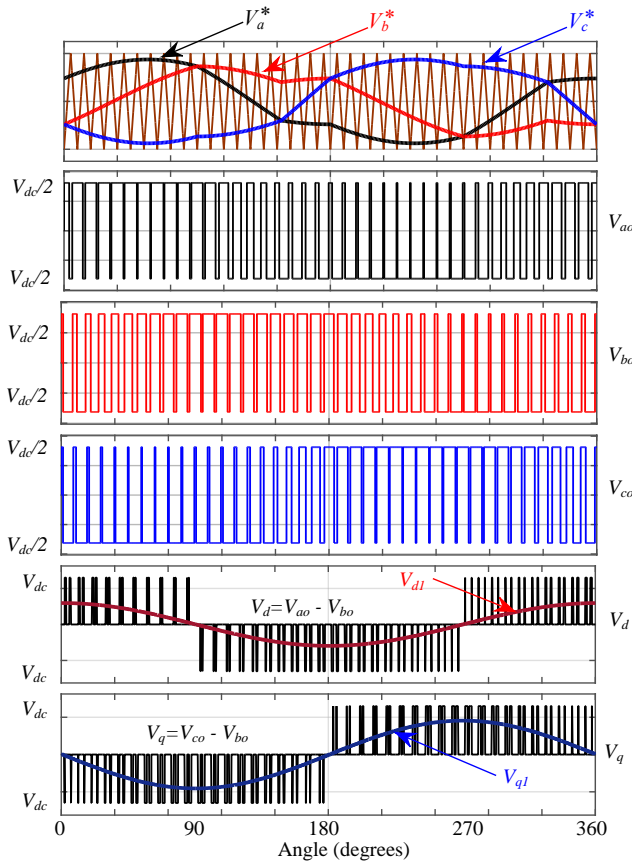


Fig. 4: Principle of the proposed unbalanced CSVPWM.

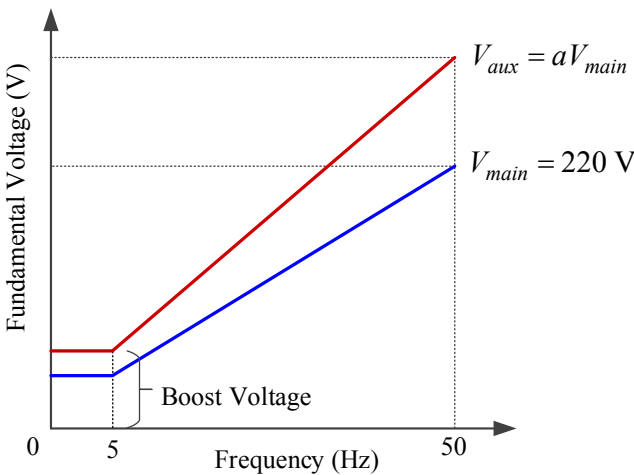


Fig. 5: Relationship between main winding voltage and auxiliary winding voltage against motor frequency.

calculation are rudimentary, including simply replicating strings, arbitrary number era, and swapping incomplete strings. The operators of GA are composed i.e. mutation, reproduction and crossover. The advantage of GA is that it is an entirely adaptable and instinctive way to deal with advancement and presents a higher likelihood of not uniting to nearby optima arrangements contrasted with conventional angle-based strategies [14].

A GA includes: a string representation of points in a search space; a set of genetic operators for generating new search points; a fitness function to evaluate the search points and a stochastic assignment to control the genetic operations. Simplicity of operation and power of effect are two main attractions of the GA approach. The approach typically has three phases [20]:

- initialization,
- evaluation,
- genetic operation.

The appropriate modified equivalent circuit parameters of the VSI-fed unsymmetrical TPIM at any condition can be estimated by using a set of measured data coupled with the use of GA as shown in Fig. 2. The data obtained from the measurement are input voltage, input current, input power, output power and speed of the motor. Data are obtained from ten conditions of motor operation at 50 Hz from no load to full load. Obtained parameter values are averaged for obtained parameter to form 10 conditions. The default parameters are  $R_{1m}$  and  $R_{1a}$  obtained from the DC test. The objective of GA is to minimize the error between the measured and calculated values of Eq. (64), Eq. (65), Eq. (66) and Eq. (67):

$$F_{objm} = \frac{1}{2} \left| \frac{I_{inputcalm}}{I_{inputmeam}} - 1 \right|^2 + \frac{1}{2} \left| \frac{P_{inputcalm}}{P_{inputmeam}} - 1 \right|^2, \tag{64}$$

$$F_{obja} = \frac{1}{2} \left| \frac{I_{inputcala}}{I_{inputmeaa}} - 1 \right|^2 + \frac{1}{2} \left| \frac{P_{inputcala}}{P_{inputmeaa}} - 1 \right|^2, \tag{65}$$

$$F_{obj} = F_{objm} + F_{obja}, \tag{66}$$

$$Fitness = F_{obj}. \tag{67}$$

Boundary values of variables which are between minimum and maximum values are shown in Tab. 1. The boundary ranges are obtained from possible values based on conventional test. Figure 6 illustrates flow chart of procedure of parameter estimation. Initially, variables are declared. Then, measured parameters like stator resistances, voltages, currents, power and speed are entered. Boundary ranges are defined. Parameter estimation procedure using GA is then processed. Finally, the optimal values of parameters are obtained. According to flow chart, the program is written in M-file of Matlab. The obtained parameters are shown in Tab. 2. Obviously, the obtained results are within boundary ranges. Table 3 illustrates parameters obtained by conventional test. Note that the rotor resistance  $R_{2m}$ ,  $R_{2a}$  obtained from the proposed GA for

equivalent circuit is higher than those obtained from conventional test. The fact is that the obtained rotor resistances are affected by skin effect. The unsymmetrical TPIM ratings are 2 HP, 220 V, 50 Hz, 4 poles.

**Tab. 1:** Initial parameter ranges of unsymmetrical TPIM for calculation.

Variable	Range
$X_{1m}$	1–3 $\Omega$
$X_{1a}$	1–20 $\Omega$
$X_{mm}$	20–100 $\Omega$
$R_{2m}$	1–4 $\Omega$
$R_{cm}$	400–1000 $\Omega$

**Tab. 2:** Parameters of TPIM from GA.

$R_{1m} = 1.203 \Omega$	$R_{1a} = 5.06 \Omega$	$X_{mm} = 82.86 \Omega$
$X_{1m} = 2.79 \Omega$	$X_{1a} = 1.20 \Omega$	$X_{ma} = 196.25 \Omega$
$R_{2m} = 3.66 \Omega$	$R_{2m} = 8.67 \Omega$	$R_{cm} = 772.05 \Omega$
$X_{2m} = 2.79 \Omega$	$X_{2m} = 6.608 \Omega$	$R_{ca} = 2.814 \Omega$

**Tab. 3:** Parameters of TPIM from conventional test.

$R_{1m} = 1.203 \Omega$	$R_{1a} = 5.06 \Omega$	$X_{mm} = 47.831 \Omega$
$X_{1m} = 1.924 \Omega$	$X_{1a} = 13.133 \Omega$	$X_{ma} = 113.289 \Omega$
$R_{2m} = 1.493 \Omega$	$R_{2m} = 3.5362 \Omega$	$R_{cm} = 596.04 \Omega$
$X_{2m} = 1.924 \Omega$	$X_{2m} = 31.107 \Omega$	$R_{ca} = 643.43 \Omega$

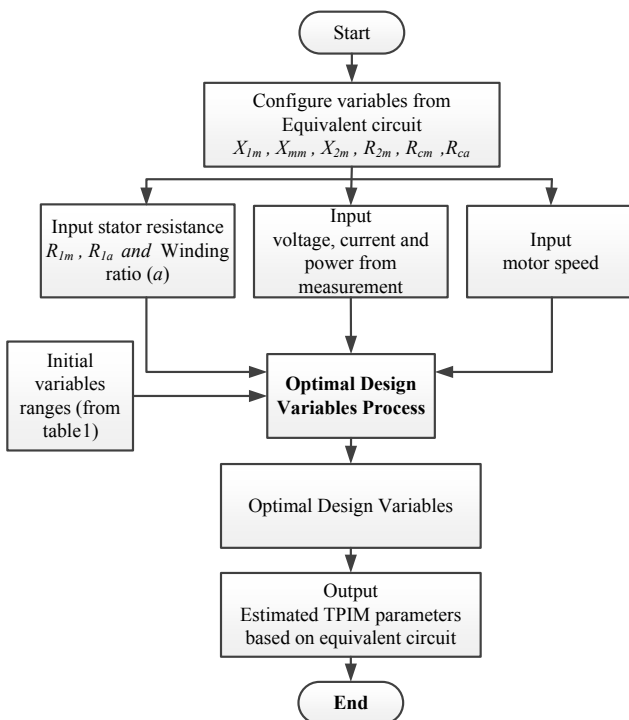


**Fig. 6:** Flow chart of unsymmetrical TPIM parameter estimation using GA.

### 3.2. Motor Loss Calculation and Synthesis of Winding Current Waveforms

In order to validate the proposed model, loss calculation and synthesis of the motor current waveforms of the three-leg VSI driven by unsymmetrical TPIM based on the supper position theorem, is performed. The harmonic spectrum of the winding voltages must be known using spectral analysis. As shown in Fig. 7 and Fig. 8, PWM voltages of both windings at rated motor frequency of 50 Hz are obtained from Matlab/Simulink and experiment, respectively. The PWM switching frequency is fixed at 5 kHz. As can be seen, the auxiliary winding voltage ( $V_q$ ) leads the main winding voltage ( $V_d$ ) by 90 degrees in accordance with Fig. 4. Simulation and experimental results are very close. Figure 9 and Fig. 10 illustrate the corresponding harmonic spectrum of winding voltages in peak value for simulation and experiment, respectively. They are in good agreement. The harmonic sidebands are at multiples of the switching frequency (i.e. 5 kHz ( $n = 100$ ), 10 kHz, 15 kHz, ...). Note that, the harmonic voltage in Fig. 9 will be used for equivalent circuits in Fig. 2 in loss calculation using Eq. (1), Eq. (2), Eq. (3), Eq. (4), Eq. (5), Eq. (6), Eq. (7), Eq. (8), Eq. (9), Eq. (10), Eq. (11), Eq. (12), Eq. (13), Eq. (14), Eq. (15), Eq. (16), Eq. (17), Eq. (18), Eq. (19), Eq. (20), Eq. (21), Eq. (22), Eq. (23), Eq. (24), Eq. (25), Eq. (26), Eq. (27), Eq. (28) and Eq. (29). The loss calculation is written in M-file of Matlab.

The fundamental peak voltage of the auxiliary winding is higher than that of the main winding for both simulation and experiment showing that the supplied voltages of the unsymmetrical TPIM are unbalanced. The fundamental voltage ratio of the auxiliary winding and the main winding is approximately 1.54, 1.55 for simulation and experiment, respectively. These values are very close to the turns ratio ( $a = 1.539$ ) in accordance with Eq. (51). The known harmonic voltages of windings are used for input voltages in equivalent circuits. In this work, the maximum order of harmonics of 500 is selected for consideration of synthesized currents and total loss since the harmonic impedance at this harmonic frequency is high enough to make the zero harmonic current. Then, the harmonics for all 500 order of winding currents are calculated by using Eq. (9) and Eq. (22) for main and auxiliary winding currents, respectively.

Figure 11 and Fig. 12 show the resultant frequency spectrum of winding currents calculated from equivalent circuits which parameters are obtained by conventional test and the proposed GA, respectively. Harmonic currents are somewhat small due to high harmonic impedances. Figure 13 illustrates the corresponding harmonic currents of the measured current

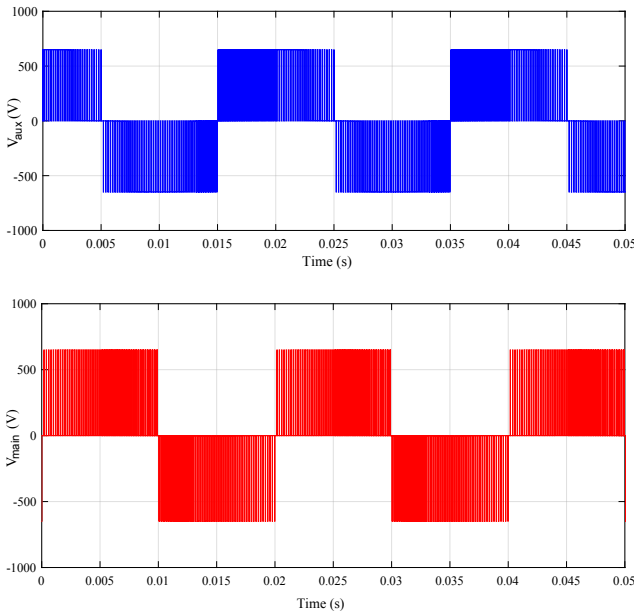


Fig. 7: Simulated PWM voltages of motor windings.

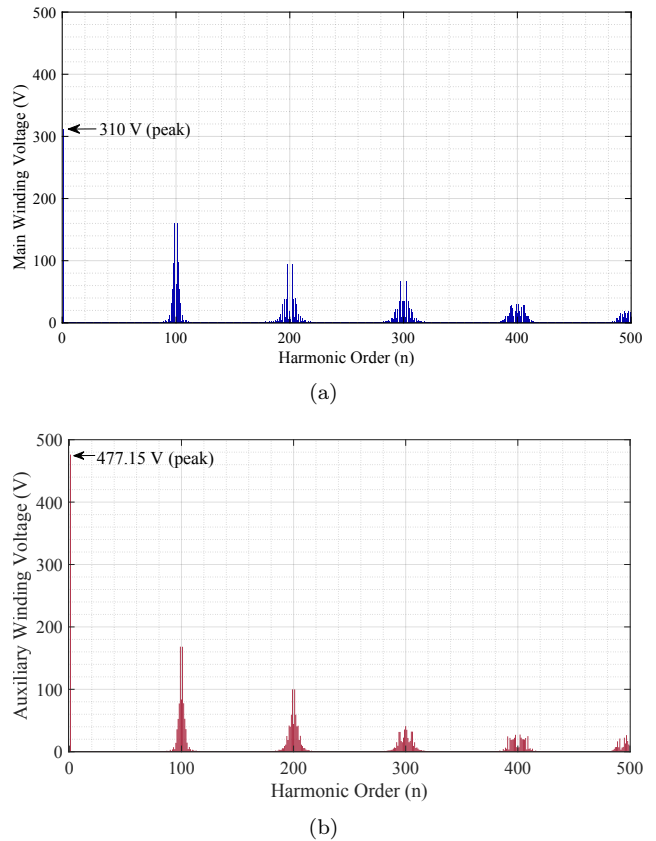


Fig. 9: Corresponding harmonic spectra of simulated voltages: (a) main winding voltage, (b) auxiliary winding voltage.

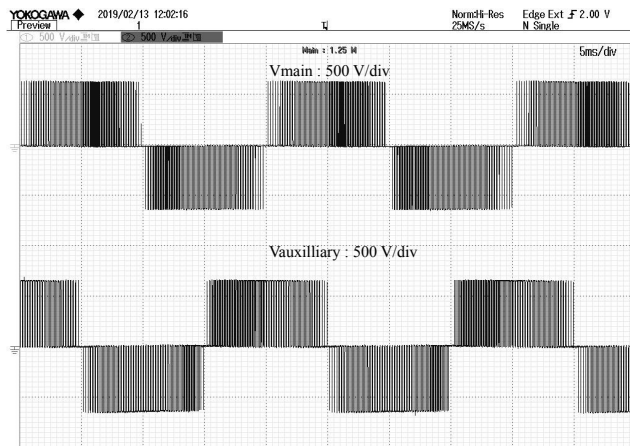
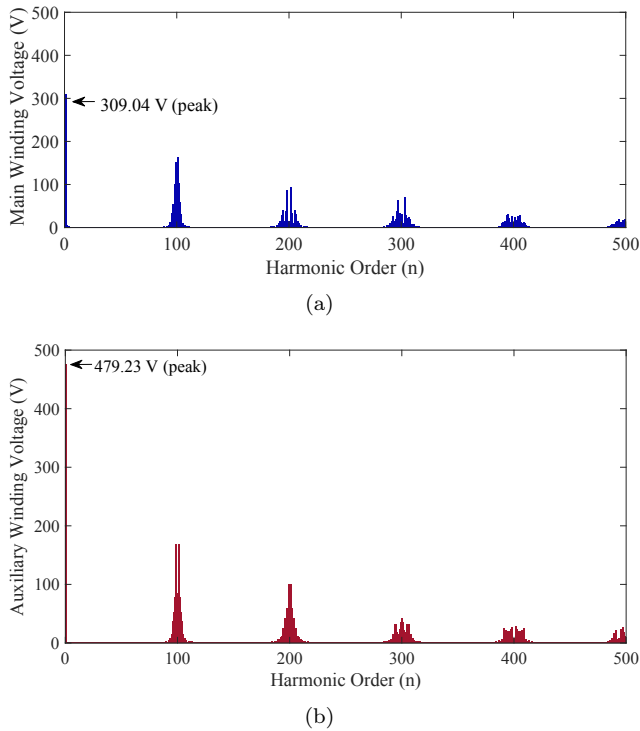


Fig. 8: Measured motor winding voltages.

waveforms. The first harmonic sidebands at the switching frequency (i.e.  $n = 100$ ,  $f = 5$  kHz) are dominant. Apparently for obtained parameters by conventional test, resultant fundamental currents of main and auxiliary windings are significantly higher than those for the measurement. Resultant fundamental currents of main and auxiliary windings for obtained parameters by the proposed GA are much closer to the corresponding fundamental currents from the measurement than those for obtained parameters by conventional test as shown in Fig. 11, Fig. 12 and Fig. 13. These results show that the parameters obtained by the proposed GA for equivalent circuits are more accurate since the proposed GA uses data sets of actual motor operation resulting in obtained parameters which could take in to account skin effect.

After that, the resultant harmonic currents from frequency domain are transformed into time domain quantity in order to synthesize current waveforms. As shown in Fig. 14 and Fig. 15, the amplitudes of main and auxiliary winding currents for parameters obtained by conventional test are much higher than those for parameters obtained by the proposed GA and the measurement. The amplitudes and ripple of main and auxiliary winding currents for parameters obtained by the proposed GA and the measurement are in good agreement. The amplitudes of both measured winding currents are almost equal which confirms that with unbalanced two-phase voltages to compensate for asymmetry of parameters, the currents of both windings of the unsymmetrical TPIM are forced to be equal. Clearly the higher imbalance of both winding currents is present for the parameters obtained by conventional test when compared to the parameters obtained by the proposed GA. This confirms that the proposed GA offers more accurate parameters resulting in better prediction.



**Fig. 10:** Corresponding harmonic spectrum of the measured voltages (a) for main winding, (b) for auxiliary winding.

### 3.3. Simulation Model

The dynamic model excluding core loss as mentioned before is used in Matlab/Simulink which tool blocks are available [22] as shown in Fig. 17.

The three-leg VSI-fed unsymmetrical TPIM is implemented in Matlab/Simulink for verifying dynamic response of currents and electromagnetic torque with parameters obtained by conventional test and the proposed GA. The proposed system consists of subsystem of generating switching pattern of continuous SVPWM for controlling three IGBT leg inverter formed as IGBT modules. The DC input voltage is set at 650 V according to the experiment. The calculation of instantaneous electromagnetic torque from Eq. (45) is written in Matlab/Simulink as shown in Fig. 18. The measured voltages and currents of main winding ( $d$ -axis) and auxiliary winding ( $q$ -axis) are used for inputs of the calculation of flux linkages and electromagnetic torque for measurement.

## 4. Experimental Results and Discussion

In order to evaluate performance characteristics of an unsymmetrical two-phase induction motor, the experimental setup is developed. It consists of a three-leg

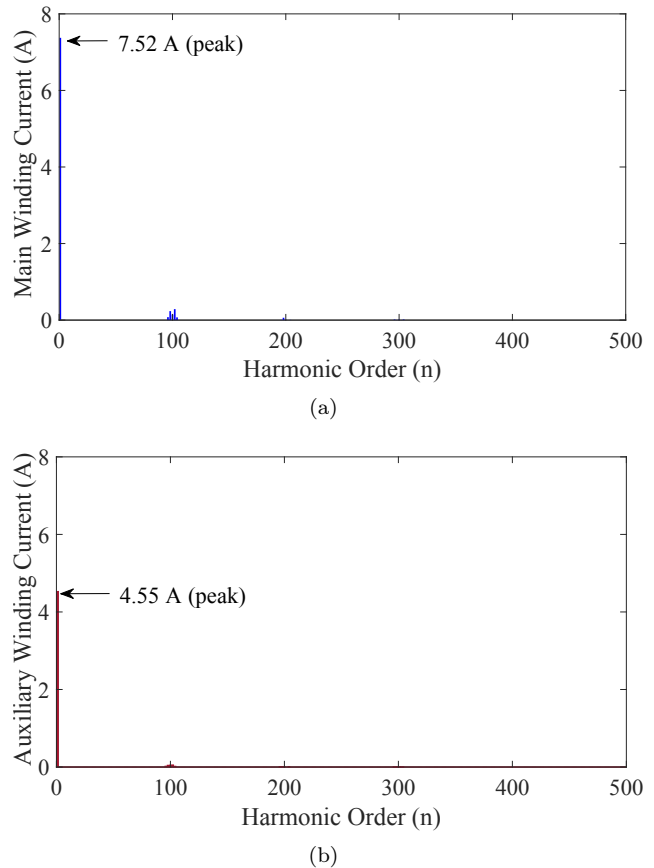


**Fig. 11:** Resultant harmonic spectrum of the winding currents with obtained parameters by conventional test (a) for main winding, (b) for auxiliary winding.

IGBT voltage source inverter with fixed 5 kHz switching frequency controlled by using a low-cost Digital Signal Controller (DSC) C2000, a DC motor drive with torque control acting as mechanical load, a TPIM modified from an existing SPIM and measurement instrument as shown in Fig. 19 and Fig. 20 for the overall block diagram of the proposed system and corresponding photograph, respectively. The DSC generates unbalanced SVPWM signals for IGBTs in the three-leg VSI via gate drivers. The DC voltage of 650 V is used to obtain the relation between winding voltages and frequency according to Fig. 5. The inverter frequency can be adjusted continuously in a wide range. The power input is measured by using an accurate power analyzer. The output power is multiplication of load torque and speed. The load torque and motor speed are measured by a torque transducer based on strain gauge and a high-resolution encoder, respectively. The measured losses are calculated from the difference between input power and output power. Dynamic response is recorded by a digital oscilloscope in conjunction with Matlab/Simulink for torque calculation.

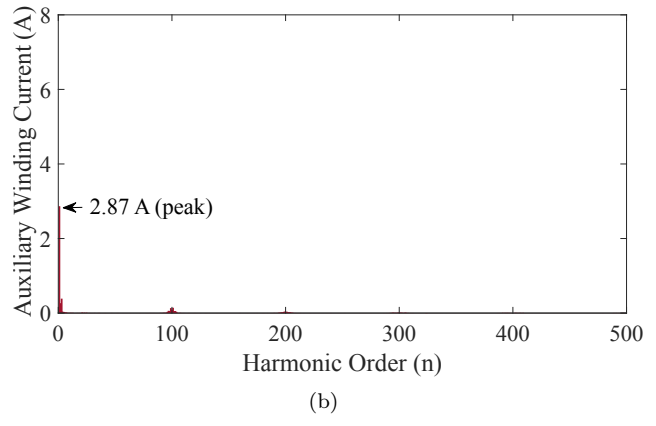
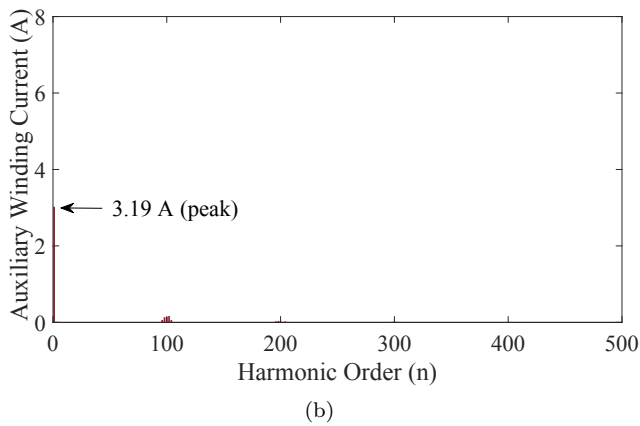
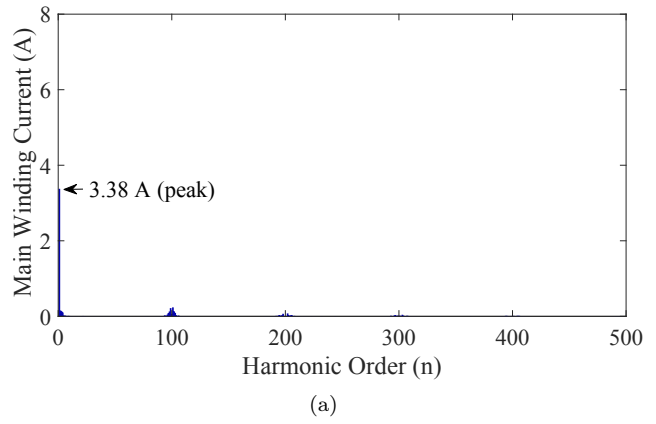
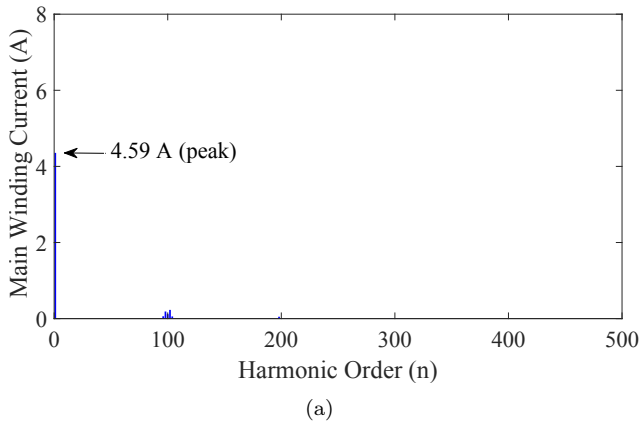


**Fig. 12:** Resultant harmonic spectrum of the winding currents with obtained parameters by the proposed GA. (a) for main winding, (b) for auxiliary winding.

**Fig. 13:** Corresponding harmonic spectrum of the measured currents (a) for main winding, (b) for auxiliary winding.

### 4.1. Motor Loss

Figure 21 shows a comparison between the calculated and measured losses with variations of load torque and inverter frequency. The motor loss is calculated using the loss model with parameters obtained by the proposed GA. The calculated and measured results are in good agreement for variations in load level and inverter frequency. These results confirm that the obtained parameters from GA are accurate.

At the same inverter frequency, when increasing the load torque, the motor loss increases with almost squared load torque due to copper loss. This is the fact that the copper loss is proportional to almost squared load torque. Copper losses in stator windings and rotor bars depends on the RMS current squared, and on the resistances (i.e.  $I_{rms}^2 R$ ). The motor current is approximately proportional to the load torque. At the same load torque when increasing the frequency, the motor loss increases due to an increase in core loss and copper loss due to skin effect. Although the inverter frequency changes, the ratio of  $V \cdot Hz^{-1}$  is constant, thus constant flux. As shown in Eq. (31), the core loss increases with squared motor frequency due to hysteresis

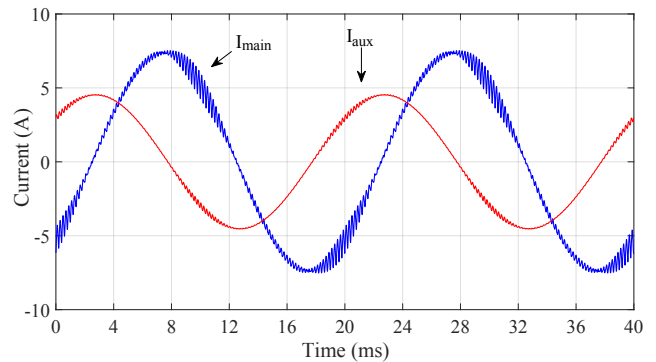


**Fig. 14:** Synthesized currents of both windings with obtained parameters by conventional test.

and eddy current losses. As well known, the core loss is independent of load level except saturation occurrence. Figure 22 illustrates a comparison of the motor loss between different methods at inverter frequency of 50 Hz with variation in load level. The motor loss calculated by Matlab/Simulink is much far lower than that of the experiment. The reason is that the resistance representing core loss is absent in the dynamic motor model. The motor loss calculated from the equivalent circuits which parameters are obtained from conventional test is significantly lower than the experiment. This is be-

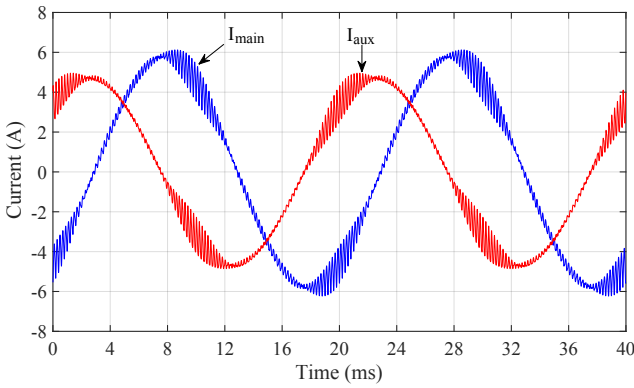


Fig. 15: Synthesized currents of both windings with obtained parameters by the proposed GA.

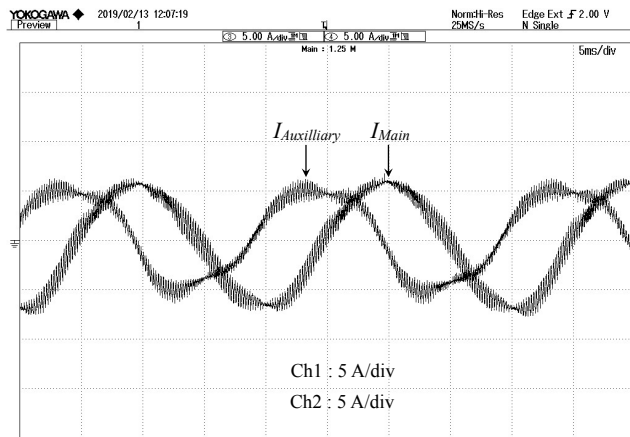


Fig. 16: Measured currents of both windings.

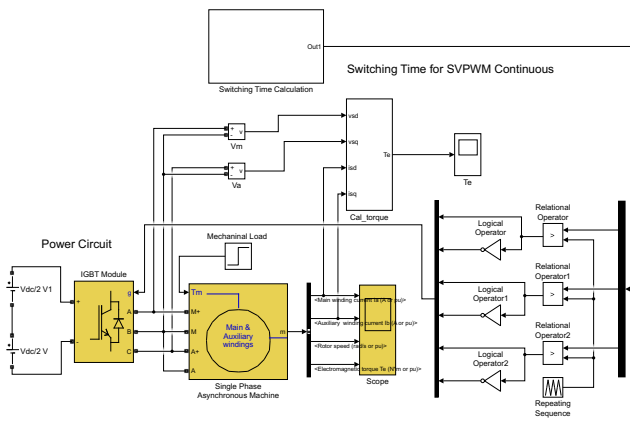


Fig. 17: Simulation model with Matlab/Simulink.

cause the rotor resistance referred to the stator side is lower than the accurate value. The motor loss calculated from the equivalent circuits which parameters are obtained from the proposed GA is almost coincide with the measured loss. The reason is that the proposed GA offers the accurate parameters particularly rotor resistances since the skin effect is taken in to account resulting in higher rotor resistance values when compared with the conventional test as shown in Tab. 2 and Tab. 3.

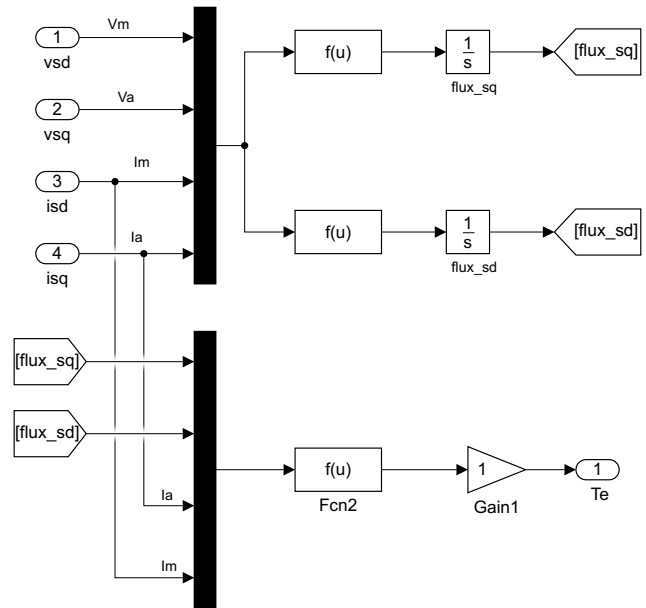


Fig. 18: Torque calculation block implemented in Matlab/Simulink.

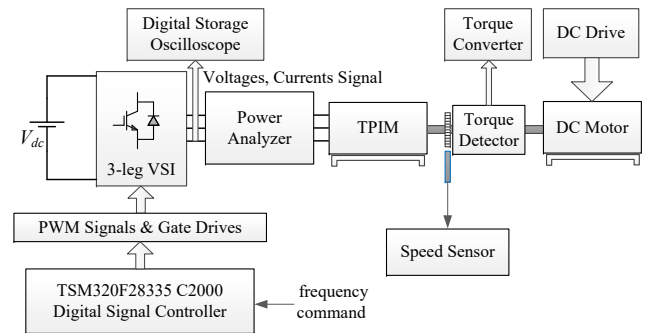


Fig. 19: Overall block diagram of the proposed system.

Another confirmation of a good accuracy of the proposed model in loss prediction at low frequency can be seen in Fig. 23. The calculated motor loss with the proposed parameters is still very close to the measured one with variation in load level.

### 4.2. Dynamic Response Performance

Figure 24, Fig. 25 and Fig. 26 illustrate dynamic response of winding currents for various methods during start up with soft start without load. Note that at the low inverter frequency, the voltage boost is added to improve starting performance in which the relationship between the fundamental voltages and inverter frequency is shown in Fig. 5. The parameters obtained by the proposed GA and conventional test are used in dynamic model available in Matlab/Simulink. The winding currents during a steady-state condition for obtained parameters by the proposed GA are close to those for the experiment. During start-up, there are no

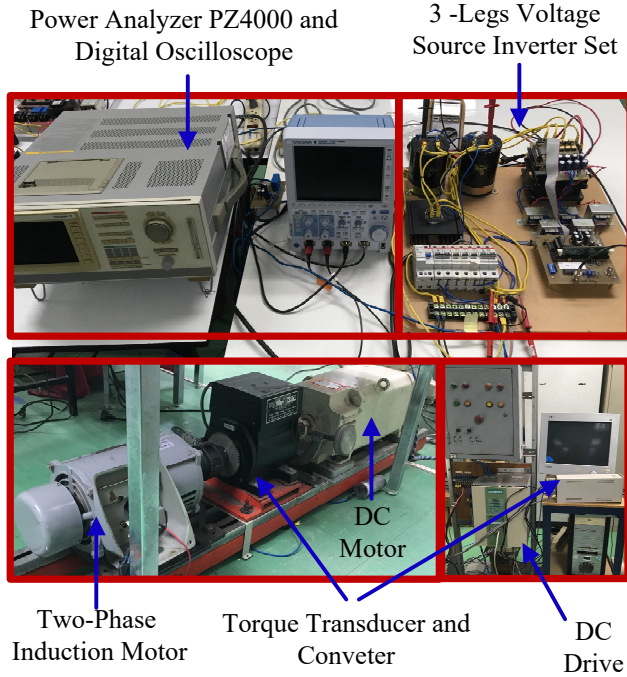


Fig. 20: Photograph of experimental setup.

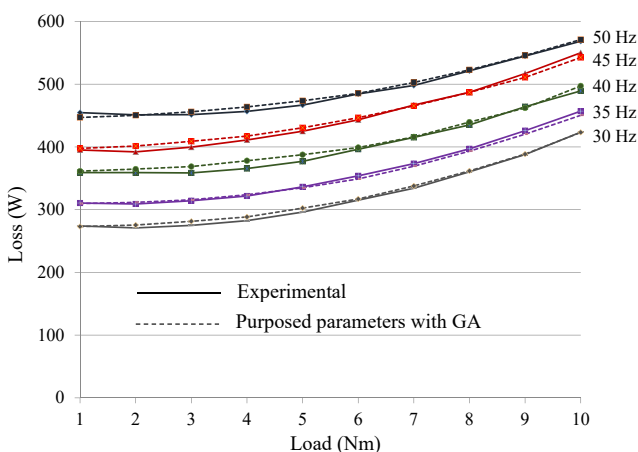


Fig. 21: Comparison of loss between experiment and calculation with variation of load and inverter frequency.

noticeable differences for peak stator winding currents among these methods. Figure 27 and Fig. 28 show the simulation results of electromagnetic torque using Matlab/Simulink during both start-up and steady-state conditions for obtained parameters by the conventional test and the proposed GA, respectively. Figure 29 shows the measured electromagnetic torque obtained from measured voltages and currents according to Fig. 18. Apparently, the peak and ripple of simulated electromagnetic torque for obtained parameters by the proposed GA and the peak and ripple of the measured electromagnetic torque are in good agreement. The electromagnetic torque ripple during the steady-state conditions for obtained parameters by the conventional test is higher than that for those methods. The results have proved that the proposed GA offers better per-

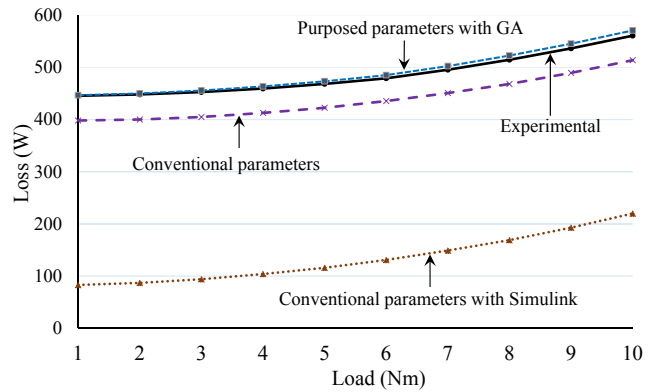


Fig. 22: Comparison of loss between simulations with Matlab/Simulink, calculation with loss model with obtained parameters by conventional test and GA, and measurement at inverter of 50 Hz and variation in load level.

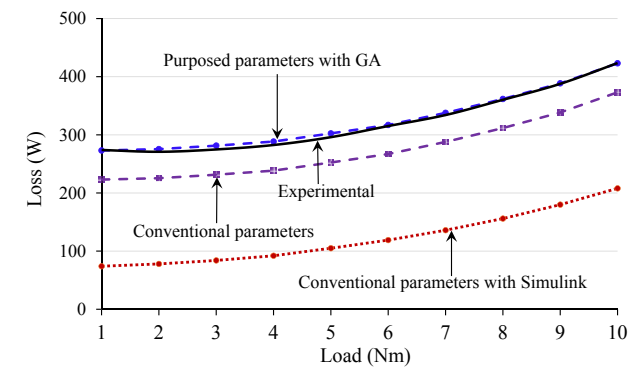
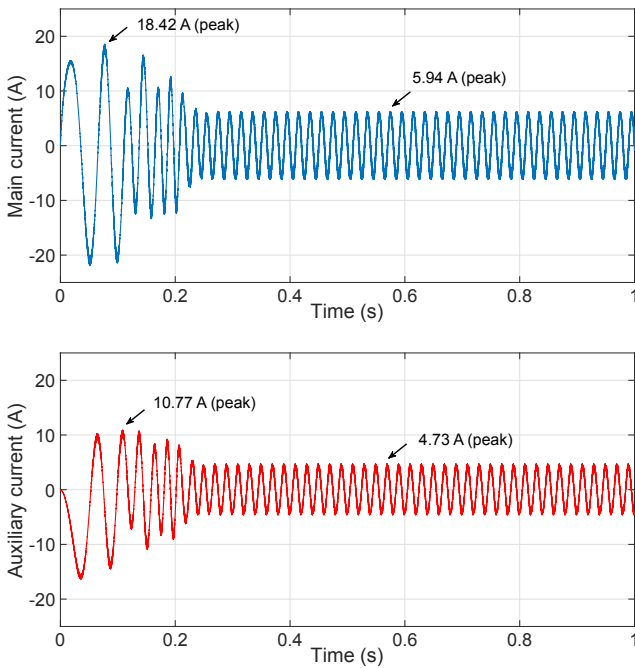


Fig. 23: Comparison of loss between simulations with Matlab/Simulink, calculation with loss model with obtained parameters by conventional test and GA, and measurement at inverter of 30 Hz and variation in load level.

formance in prediction when compared to the conventional test in identifying the motor parameters for loss model and dynamic model.

## 5. Conclusion

This paper has proposed the evaluation method of performance characteristics of an unsymmetrical TPTM driven by a two-phase three-leg VSI. The proposed loss model including fundamental and harmonic losses is based on equivalent circuits. The motor parameters for the equivalent circuits are obtained by a GA technique. The synthesized currents have been performed based on the proposed equivalent circuits using transformation from frequency domain to time domain. The measured and synthesized currents are in good agreement. The loss characteristics under variations in inverter frequency and load torque level are in accordance with the theoretical ones. The results of dy-



**Fig. 24:** Simulated starting currents of main and auxiliary windings with obtained parameters by conventional test.

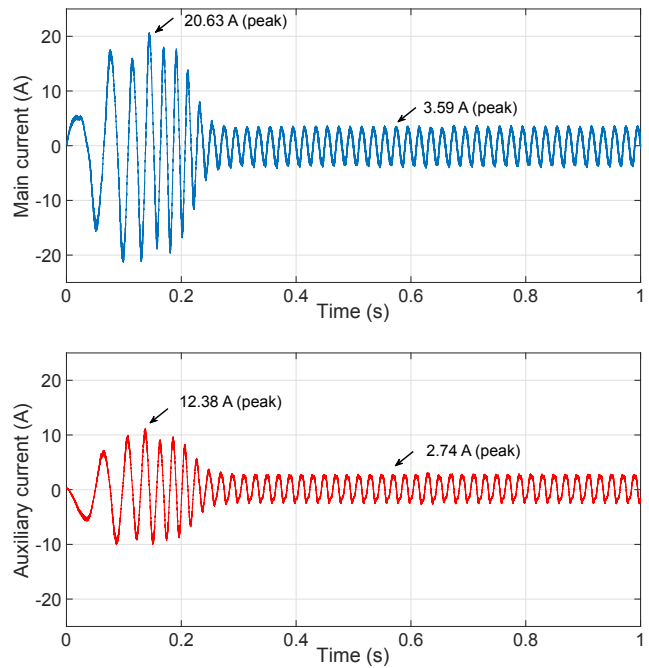


**Fig. 26:** Measured starting currents of main and auxiliary windings.

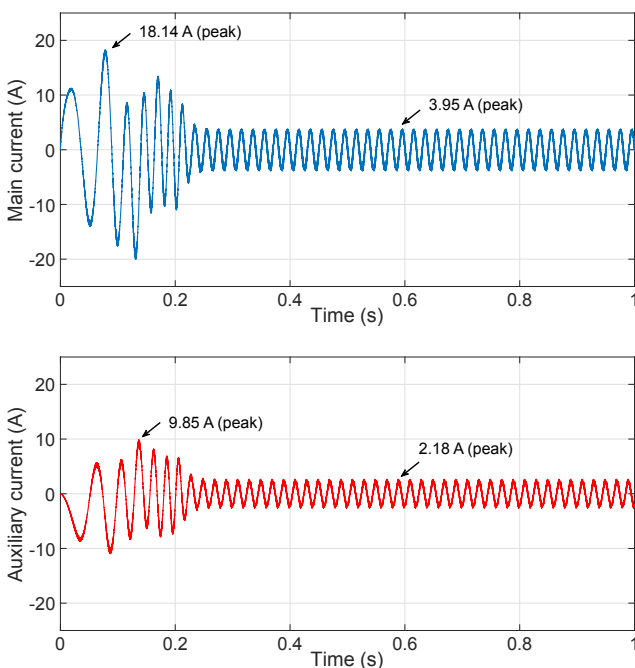


**Fig. 25:** Simulated starting currents of main and auxiliary windings with obtained parameters by GA.

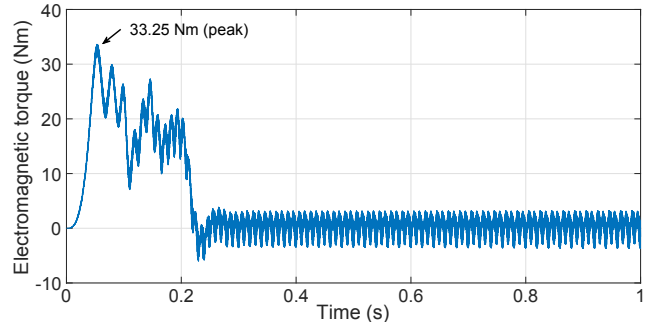


**Fig. 27:** Simulated electromagnetic torque with obtained parameters by conventional test during start-up with soft start.

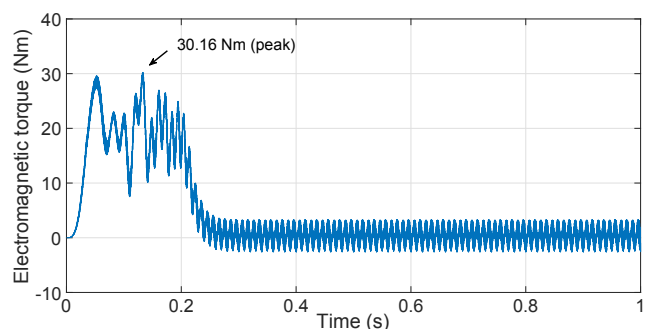


**Fig. 28:** Simulated electromagnetic torque with obtained parameters by GA during start-up with soft start.

dynamic response of currents and electromagnetic torque during start up to steady state for parameter obtained by the proposed GA and for the measurement are in accordance. With these results, the motor parameters obtained by the proposed GA are validated. The proposed model offers a good accuracy in loss prediction since parameters by GA are searched based on some

realistic data of motor test. As a consequence, some effects like skin effect and saturation are taken into account. The proposed work is useful for motor design

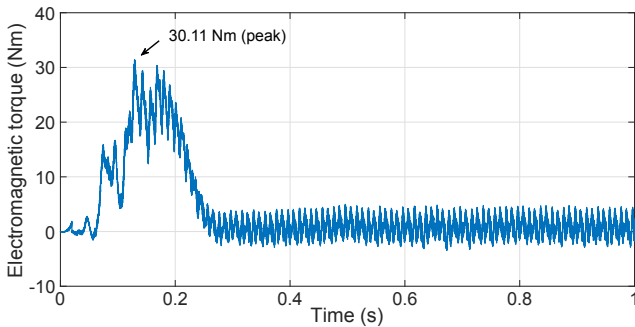


**Fig. 29:** Measured electromagnetic torque during start-up with soft start.

and control to meet achievement of high efficiency and good performance.

## Acknowledgment

The authors gratefully acknowledge the promotion of energy conservation, Energy Policy and Planning Office (EPPO), Ministry of Energy and Rajamangala University of Technology Tawan-Ok, Thailand for financial support in terms of research and scholarship for Mr. Prayad Kongsuk.

## References

- [1] PIYARAT, W., P. HOTHONGKHAM, C. CHARUMIT and V. KINNARES. Simple Speed Control of an Asymmetrical Type Two-Phase Induction Motor Drive. In: *ECTI International Conference on Electrical Engineering/Electronics, Computer, Telecommunications and Information Technology*. Chiang Mai: IEEE, 2010, pp. 274–278. ISBN 978-1-4244-5606-2.
- [2] BLAABJERG, F., F. LUNGEANU, K. SKAUG and M. TONNES. Two-phase induction motor drives. *IEEE Industry Applications Magazine*. 2004, vol. 10, iss. 4, pp. 24–32. ISSN 1077-2618. DOI: 10.1109/MIA.2004.1311160.
- [3] KINNARES, V. and C. CHARUMIT. Modulating Functions of Space Vector PWM for Three-Leg VSI-Fed Unbalanced Two-Phase Induction Motors. *IEEE Transactions on Power Electronics*. 2009, vol. 24, iss. 4, pp. 1135–1139. ISSN 0885-8993. DOI: 10.1109/TPEL.2008.2011906.
- [4] KUMSUWAN, Y., S. PREMRUDEEP-REECHACHARN and V. KINNARES. A Carrier-Based Unbalanced PWM Method for Four-Leg Voltage Source Inverter Fed Unsymmetrical Two-Phase Induction Motor. *IEEE Transactions on Industrial Electronics*. 2013, vol. 60, iss. 5, pp. 2031–2041. ISSN 0278-0046. DOI: 10.1109/TIE.2012.2228138.
- [5] PIYARAT, W., P. HOTHONGKHAM and V. KINNARES. Performance comparison of an asymmetrical parameter type two-phase induction motor supplied with balanced and unbalanced phase voltages. In: *ECTI International Conference on Electrical Engineering/Electronics, Computer, Telecommunications and Information Technology*. Chiang Mai: IEEE, 2010, pp. 264–268. ISBN 978-1-4244-5606-2.
- [6] ZAHEDI, B. and S. VAEZ-ZADEH. Efficiency Optimization Control of Single-Phase Induction Motor Drives. *IEEE Transactions on Power Electronics*. 2009, vol. 24, iss. 4, pp. 1062–1070. ISSN 0885-8993. DOI: 10.1109/TPEL.2008.2011639.
- [7] ZAHEDI, B. and S. VAEZ-ZADEH. Analysis of Electrical Loss in Single Phase Induction Motors. In: *International Electric Machines & Drives Conference*. Antalya: IEEE, 2007, pp. 1621–1625. ISBN 1-4244-0742-7. DOI: 10.1109/IEMDC.2007.383672.
- [8] MADEMLIS, C., I. KIOSKERIDIS and T. THEODOULIDIS. Optimization of single-phase induction Motors-part I: maximum energy efficiency control. *IEEE Transactions on Energy Conversion*. 2005, vol. 20, iss. 1, pp. 187–195. ISSN 0885-8969. DOI: 10.1109/TEC.2004.842386.
- [9] MADEMLIS, C., I. KIOSKERIDIS and T. THEODOULIDIS. Optimization of single-phase induction Motors-part II: magnetic and torque performance under optimal control. *IEEE Transactions on Energy Conversion*. 2005, vol. 20, iss. 1, pp. 196–203. ISSN 0885-8969. DOI: 10.1109/TEC.2004.842383.
- [10] CHAT-UTHAI, C. and P. PHUMIPHAK. Low-Intrusive Approach for Parameters Estimation of Induction Motor Using Adaptive Optimal Design Algorithm Based on On-Site Measurements. *International Review of Electrical Engineering*. 2013, vol. 8, no. 4, pp. 1162–1169. ISSN 1827-6660.
- [11] RUTCZYNSKA-WDOWIAK, K. Replacement strategies of genetic algorithm in parametric identification of induction motor. In: *22nd International Conference on Methods and Models in Automation and Robotics (MMAR)*. Miedzyzdroje: IEEE, 2017, pp. 971–975. ISBN 978-1-5386-2402-9. DOI: 10.1109/MMAR.2017.8046961.
- [12] KAMPISIOS, K., P. ZANCHETTA, C. GERADA and A. TRENTIN. Identification of In-

- duction Machine Electrical Parameters using Genetic Algorithms Optimization. In: *Industry Applications Society Annual Meeting*. Edmonton: IEEE, 2008, pp. 1–7. ISBN 978-1-4244-2278-4. DOI: 10.1109/08IAS.2008.165.
- [13] ALONGE, F., F. D'IPPOLITO, G. FERRANTE and F. M. RAIMONDI. Parameter identification of induction motor model using genetic algorithms. *IEE Proceedings - Control Theory and Applications*. 1998, vol. 145, iss. 6, pp. 587–593. ISSN 1350-2379. DOI: 10.1049/ip-cta:19982408.
- [14] PHUMIPHAK, T. and C. CHAT-UTHAI. Estimation of induction motor parameters based on field test coupled with genetic algorithm. In: *Proceedings. International Conference on Power System Technology*. Kunming: IEEE, 2002, pp. 1199–1203. ISBN 0-7803-7459-2. DOI: 10.1109/ICPST.2002.1047592.
- [15] SRIDHARA RAO, G. and S. HOSIMIN THILAGAR. A Novel Method for the Determination of Stray Load Losses of Induction Motor Using Genetic Algorithm. In: *Canadian Conference on Electrical and Computer Engineering. Toward a Caring and Humane Technology (CCECE)*. Montreal: IEEE, 2003, pp. 259–262. ISBN 0-7803-7781-8. DOI: 10.1109/CCECE.2003.1226391.
- [16] BOGLIETTI, A., A. CAVAGNINO, L. FERRARIS and M. LAZZARI. Impact of the Supply Voltage on the Stray-Load Losses in Induction Motors. *IEEE Transactions on Industry Applications*. 2010, vol. 46, iss. 4, pp. 1374–1380. ISSN 0093-9994. DOI: 10.1109/TIA.2010.2049721.
- [17] KONGSUK, P., W. PROMKHUN and V. KINNARES. Measured Loss Evaluation of Asymmetrical Parameter Type Two-Phase Induction Motor Supplied with a Three-leg Voltage Source Inverter. In: *17th International Conference on Electrical Machines and Systems (ICEMS)*. 2014, Hangzhou: IEEE, 2014, pp. 2561–2566. ISBN 978-1-4799-5162-8. DOI: 10.1109/ICEMS.2014.7013933.
- [18] KONGSUK, P. and V. KINNARES. Loss Modeling of Three-Leg Voltage Source Inverter fed Asymmetrical Two-Phase Induction Motor. In: *18th International Conference on Electrical Machines and Systems (ICEMS)*. Pattaya: IEEE, 2015, pp. 732–736. ISBN 978-1-4799-8805-1. DOI: 10.1109/ICEMS.2015.7385130.
- [19] GHIAL, V. K., L. M. SAINI and J. S. SAINI. Parameter Estimation of Permanent-Split Capacitor-Run Single-Phase Induction Motor Using Computed Complex Voltage Ratio. *IEEE Transactions on Industrial Electronics*. 2014, vol. 61, iss. 2, pp. 682–692. ISSN 0278-0046. DOI: 10.1109/TIE.2013.2253067.
- [20] KAMEPALLI, H. B. The optimal basics for GAs. *IEEE Potentials*. 2001, vol. 20, iss. 2, pp. 25–27. ISSN 0278-6648. DOI: 10.1109/45.954645.
- [21] HUANG, K. S., Q. H. WU and D. R. TURNER. Effective Identification of Induction Motor Parameters Based on Fewer Measurements. *IEEE Transactions on Energy Conversion*. 2002, vol. 17, iss. 1, pp. 55–60. ISSN 0885-8969. DOI: 10.1109/60.986437.
- [22] ONG, C. M. *Dynamic Simulation of Electric Machinery Using MATLAB/SIMULINK*. 1st ed. Upper Saddle River: Prentice Hall, 1997. ISBN 978-0-1372-3785-2.

## About Authors

**Prayad KONGSUK** was born in Surin, Thailand. He received the B.Eng. degree in electrical engineering from Rajamangala University of Technology Isan, Nakhonratchasima, Thailand and M.Eng. degree in electrical engineering from King Mongkut's University of Technology North Bangkok, Bangkok, Thailand. He is currently student of the doctor's degree in electrical engineering at King Mongkut's Institute of Technology Ladkrabang. His research interests include energy conversion, power electronics and drives.

**Vijit KINNARES** (Member of IEEE) was born in Sakon Nakhon, Thailand. He received the B.Eng. and M.Eng. degree in electrical engineering from King Mongkut's Institute of Technology Ladkrabang, Bangkok, Thailand, and received the Ph.D. degree in electrical engineering from University of Nottingham, England. Currently, he is an Assoc. Professor at King Mongkut's Institute of Technology Ladkrabang. His research interests include renewable energy systems, power electronics and drives.

**Phunyaphat PHUMIPHAK** was born in Bangkok, Thailand. He received the B.Eng., M.Eng. and D.Eng. degree in electrical engineering from the King Mongkut's Institute of Technology Ladkrabang in 1996, 2000 and 2014 respectively. Currently, he is an Asst. Professor at Mahanakorn University of Technology. His research interests include electrical machines, design optimization.

## Appendix A

### Nomenclature

$V_{mn}$	main winding voltage at order $n$ ,	$a$	turns ratio of aux. and main windings,
$V_{an}$	auxiliary winding voltage at order $n$ ,	$V_d, V_q$	main, auxiliary winding voltage,
$I_{mn}$	main winding current at order $n$ ,	$I_d, I_q$	main, auxiliary winding current,
$I_{an}$	auxiliary winding current at order $n$ ,	$v_{sd}^s, v_{sq}^s$	$d, q$ axis stator voltage component,
$Z_{mn}$	main winding impedances at order $n$ ,	$i_{sd}^s, i_{sq}^s$	$d, q$ axis stator current component,
$Z_{an}$	auxiliary winding impedances at order $n$ ,	$\lambda_{sd}^s, \lambda_{sq}^s$	$d, q$ axis stator flux component,
$n$	order of harmonics,	$\lambda_{rd}^s, \lambda_{rq}^s$	$d, q$ axis rotor flux component,
$s_n$	$n^{\text{th}}$ order harmonic slip,	$R_{sd}, R_{sq}$	$d, q$ axis stator resistance,
$R_{cm}$	main core loss equivalent resistance,	$R_r$	rotor resistance,
$R_{ca}$	auxiliary core loss equivalent resistance,	$L_{sd}, L_{sq}$	$d, q$ axis stator self-inductance,
$P_{Cus}, P_{Cur}$	stator copper loss, rotor copper loss,	$L_r$	rotor self-inductance,
$P_{Fe}$	core loss,	$M_{srd}, M_{srq}$	$d, q$ axis mutual inductance,
$P_{in}$	input power,	$\omega_r$	rotor angular speed in $\text{rad}\cdot\text{s}^{-1}$ ,
$P_m$	mechanical power,	$T_e, T_m$	electromagnetic, mechanical torque,
		$P$	number of pole pairs,
		$J$	rotor moment of inertia,
		$B$	viscous friction coefficient.